IEEE Photonics Journal
An IEEE Photonics Society Publication

Open Access

Sidewall Profile Dependent Nanostructured Ultrathin Solar Cells With Enhanced Light Trapping Capabilities

Volume 12, Number 1, February 2020

Tangyou Sun
Jie Tu
Le Cao
Tao Fu
Qi Li
Fabi Zhang
Gongli Xiao
Yonghe Chen
Haiou Li
Xingpeng Liu
Zhiqiang Yu
Yue Li
Wenning Zhao

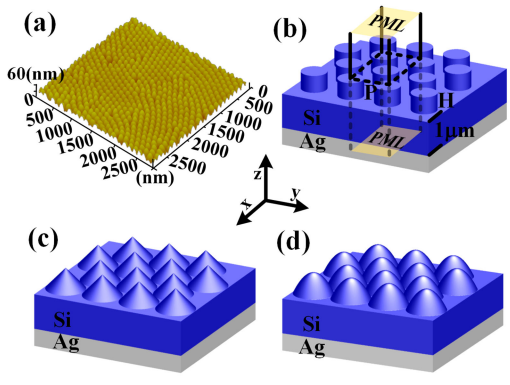

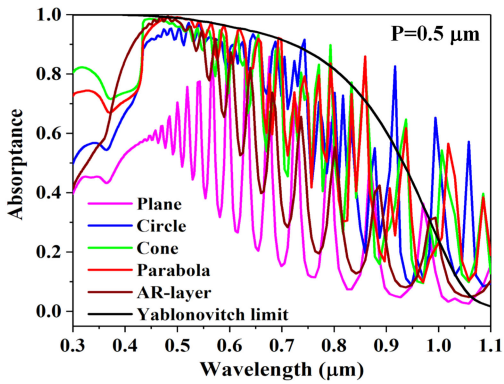

DOI: 10.1109/JPHOT.2019.2961566

IEEE photonics SOCIETY
IEEE

Sidewall Profile Dependent Nanostructured Ultrathin Solar Cells With Enhanced Light Trapping Capabilities

Tangyou Sun,[1] Jie Tu,[1] Le Cao,[1] Tao Fu,[1] Qi Li,[1] Fabi Zhang,[1] Gongli Xiao,[1] Yonghe Chen,[1] Haiou Li,[1] Xingpeng Liu,[1] Zhiqiang Yu,[2] Yue Li,[1] and Wenning Zhao[3]

[1]Guangxi Key Laboratory of Precision Navigation Technology and Application, Guilin University of Electronic Technology, Guilin 541004, China
[2]School of Electrical and Information Engineering, Guangxi University of Science and Technology, Liuzhou 545006, China
[3]Institute of Engineering Research, Jiangxi University of Science and Technology, Ganzhou 341000, China

DOI:10.1109/JPHOT.2019.2961566

Manuscript received November 21, 2019; revised December 16, 2019; accepted December 18, 2019. Date of publication December 23, 2019; date of current version February 28, 2020. This work was supported in part by the National Natural Science Foundation of China under Grants 11965009, 61874036, 61805053, and 61764001, in part by the Guangxi Innovation Research Team Project under Grant 2018GXNSFGA281004, in part by the Guangxi Science and Technology Project under Grants AD18281030, AD18281034, and AD18281037, in part by the Guangxi Natural Science Foundation under Grants 2016GXNSFDA380021, 2017GXNSFAA198164, 2018GXNSFBA050052, and 2018GXNSFBA281152, and in part by the Guangxi Key Laboratory of Precision Navigation Technology and Application, Guilin University of Electronic Technology under Grant DH201801. Corresponding authors: Xingpeng Liu; Wenning Zhao (e-mail: tadyliu@guet.edu.cn; zhaowenning@126.com).

Abstract: Theoretical studies of ultra-thin silicon solar cells with cylindrical, conical and parabolic surface nanostructures inherited from natural self-assembled anodic alumina oxide (NSA-AAO) were performed by finite-difference time-domain (FDTD) method. All nanostructured solar cells obtained an optimized efficiency enhancement as high as more than 33% comparing with that of the anti-reflective (AR) one. Numerical results reveal that the range of efficient structural parameters for the nanostructured (e.g., cylindrical) solar cell can be effectively enlarged as the period of the nanostructure changes from 0.1 μm to 0.5 μm. Moreover, the improvements of absorption photocurrent density (Jph) in conical and parabolic nanostructured solar cells are comparable with the cylindrical nanostructured one but less sensitive to the fill factor and structural height in the whole simulation region of 0.1–0.9 and 0–0.25 μm, respectively. Equivalent refractive index models were used to analysis the antireflection performance of surface nanostructures from the point of view of sidewall profiles. Resonance modes induced through nanostructures have greatly improved the absorptance of solar cells in broadening wavelength bands which consequently raised the Jph. This study serves as a way for the practical design and application of AAO nanostructure based high-efficiency ultra-thin solar cells.

Index Terms: Nanostructure, light trapping, solar cell.

1. Introduction

Due to the high cost and low efficiency of the traditional solar cells induced from thick absorption layers, much attention has been paid to the continually developed ultra-thin solar cells [1]–[4]. However, the light absorption of the ultra-thin silicon solar cell is greatly restricted because of the

limited layer thickness. To solve this problem, nanostructures are commonly used because of its high anti-reflection and light trapping abilities [5]–[12]. Most recently, due to the requirement of low cost and dimension controllable properties of the nanostructure, self-assembled nano-preparation method has been proposed, and the commercial value outstands in the widespread use of photovoltaic devices [13]–[16] and light-emitting diodes [17], [18]. Moreover, some achieves have shown that nanostructure with gradually changed sidewall profiles can effectively improve the optical performance of the solar cells [19]–[22]. Guan Zisheng *et al.* made an inverted pyramid structured c-Si solar cell by controlling the metal assisted chemical etching process, which improved the Jsc by 0.22 mA/cm^2 when comparing with the best positive pyramid structured c-Si solar cell [20]. Fan Zhiyong *et al.* used the pre-imprinting anodization AAO (PIA-AAO) process to prepare amorphous silicon solar cells on nano-cone plastic substrates, the light trapping efficiency reached as high as two folds of the similar planar devices [21]. Gao Pingqi *et al.* proposed a high-throughput nanosphere patterning method to form a periodic upright nanopyramid arrays on the silicon surface, resulting a 1.35 mA/cm^2 Jsc improvement by comparing with the state-of-the-art random pyramids textured one [22]. However, most of these studies are based on single morphology parameter of the structures. During our previous study, we found that multiple structural parameters should be considered together in order to optimize the efficiency of corresponding nano-structured solar cells. In this article, the relationship between nanostructured parameters (period, fill factor (the occupied area of the nanostructure divided by the whole surface area), height, etc.) of various sidewall profiles and solar cell absorption are studied base on the NSA-AAO process. Which could be of great help to the device design and the selection of fabrication process towards low cost high throughput mass production area.

In this paper, we applied cylindrical nanostructure (CDN), conical nanostructure (CCN) and parabolic nanostructure (PBN) inherited from the NSA-AAO to the surface of silicon-based solar cells through FDTD Solutions of Lumerical optical module. The relationships between the Jph (photocurrent density) and the fill factor, the period as well as the height of the nanostructured solar cells were analyzed by FDTD method. In addition, the light capture ability and internal field distribution of the corresponding nanostructured solar cells were studied. These results serve as a way to optimize the light trapping efficiency of the AAO nanostructure based solar cells.

2. Methods

Since the AAO based replication method was proposed by Masuda and Fukuda in 1995 [23], AAO has been widely used as a template to prepare various nanostructured metal, polymers, and semiconductors due to its nanoscale feature size and pore dimension tunable properties [24]–[26]. Fig. 1(a) shows a representative nanostructured array obtained from the AAO based bilayer polydimethylsiloxane (PDMS) replication scheme [27]. The triangular distributed nanostructure is totally inherited from the initial AAO template because of a 1 : 1 pattern transfer property, which means the regularity of the transferred nanostructures are determined by the growth condition of the initial AAO template [28]. To date, three representative sidewall profiles, cylinder, cone and parabola, have been realized by commonly applied nanofabrication processes (nanoimprinting, lithography, dry etching, etc.) [29]–[32], thus were chosen as the simulation models in this work as shown in Fig. 1(b), (c), (d). In order to clearly describe the simulation area, Fig. 1(e) gives top and cross-sectional views.

For the fabrication of large-pore NSA-AAO ($>$0.5 μm), despite of the non-regularity of the AAO nano-pore distribution, the burn-through issue must be overcomed because of a high-voltage anodization [18], [35], [36]. While a better efficiency enhancement of the structured opto-electronic device is usually obtained based on highly ordered nano-structures [22], [37]. Although by inviting the PIA-AAO method, highly ordered AAO can be fabricated with large-pore dimension [21], the method complexes the fabrication processes and improves the cost, which degrades the advantages that the NSA-AAO it deserves. Moreover, with respect to analysis methods, when feature size F_d of the nanostructure satisfies $F_d < \lambda/n$ (where λ is the light wavelength and n is the refractive index of the material under consideration), the sub-wavelength structure (SWS) and equivalent

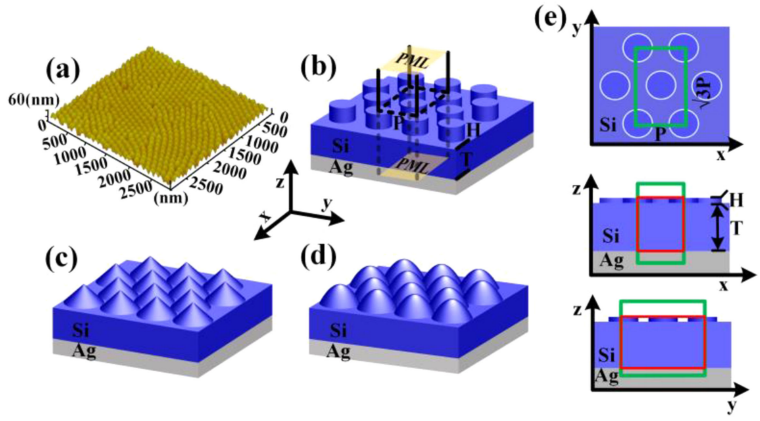

Fig. 1. (a) Oblique view of the nanostructured array under atomic force microscopy, prepared by PDMS replication method. Simulation models with (b) cylindrical sidewall profile, (c) conical sidewall profile and (d) parabolic sidewall profile, (e) top view and cross-sectional view of simulation configuration for cylindrical nanostructured solar cell, in which the green rectangle is the simulation area and the red one is the monitor. Each model uses 1 μm thick of c-si as the absorption layer and a 0.5 μm thick real silver as the back-reflector, the n-k-data of Si and Ag come from Handbook of Optical Constants of Solids [33] and CRC handbook of Chemistry & Physics [34], respectively.

refractive index models can be used for the antireflection study of the nanostructured surface. While for an even larger F_d, the photonic crystal or geometrical optics effects will dominate, and numerous studies regarding $F_d > 0.5$ μm have been carried out based on various nanofabrication methods [22], [38], [39]. Therefore, under all these considerations, the simulation period of the structure ranges from 0.1 μm to 0.5 μm is chosen in this paper. The symmetrical two adjacent triangular lattices are used as the smallest simulation area, as shown by the dashed lines of Fig. 1(b) [18]. The simulation area of Fig. 1(b), Fig. 1(c) and Fig. 1(d) are the same as Fig. 1(e). In the simulation, Jph was separately calculated via the plane wave source ranging from 0.3 μm to 1.1 μm under 0-degree and 90-degree polarizations. The average of these two-polarization dependent Jph was used to define the results of the unpolarized sunlight. To simplify the simulation, the asymmetric and symmetric boundary conditions were respectively applied to the X and Y axes when the light source was 0-polarized. When light source polarization was 90 degrees, the boundary conditions of the X and Y axes were opposite to those of 0-polarized and the z-axis adopted perfectly matched layer boundary conditions [40]. The calculation of Jph was used to quantitatively measure the light trapping ability of nanostructured solar cell under solar illumination [41]. Reflectivity and absorptance spectra of the simulation are available through the frequency-domain field and power monitors in FDTD solutions. The grid accuracy of the simulations for x, y and z are 0.008 μm, 0.008 μm and 0.005 μm respectively, which ensure the convergence and correctness of the results. The Jph under the condition of solar radiation AM1.5 can be obtained by the following formula [42]:

$$J_{ph} = e \int_{300\,nm}^{1100\,nm} \frac{\lambda}{hc} A(\lambda) I_{AM1.5}(\lambda) d\lambda \tag{1}$$

$$A(\lambda) = 1 - R(\lambda) - T(\lambda) \tag{2}$$

where $A(\lambda)$ represents the absorption of solar energy by silicon, e is the electron charge, h is the Planck constant, c is the speed of light in vacuum, $I_{AM1.5}(\lambda)$ is the incident light spectrum AM1.5.

3. Results and Discussions

To study the light trapping performance of CDN, CCN, and PBN, the relationships between structural parameters and Jph was obtained by varying P (Period), H (Height) and F (Fill factor). The results are shown in Fig. 2.

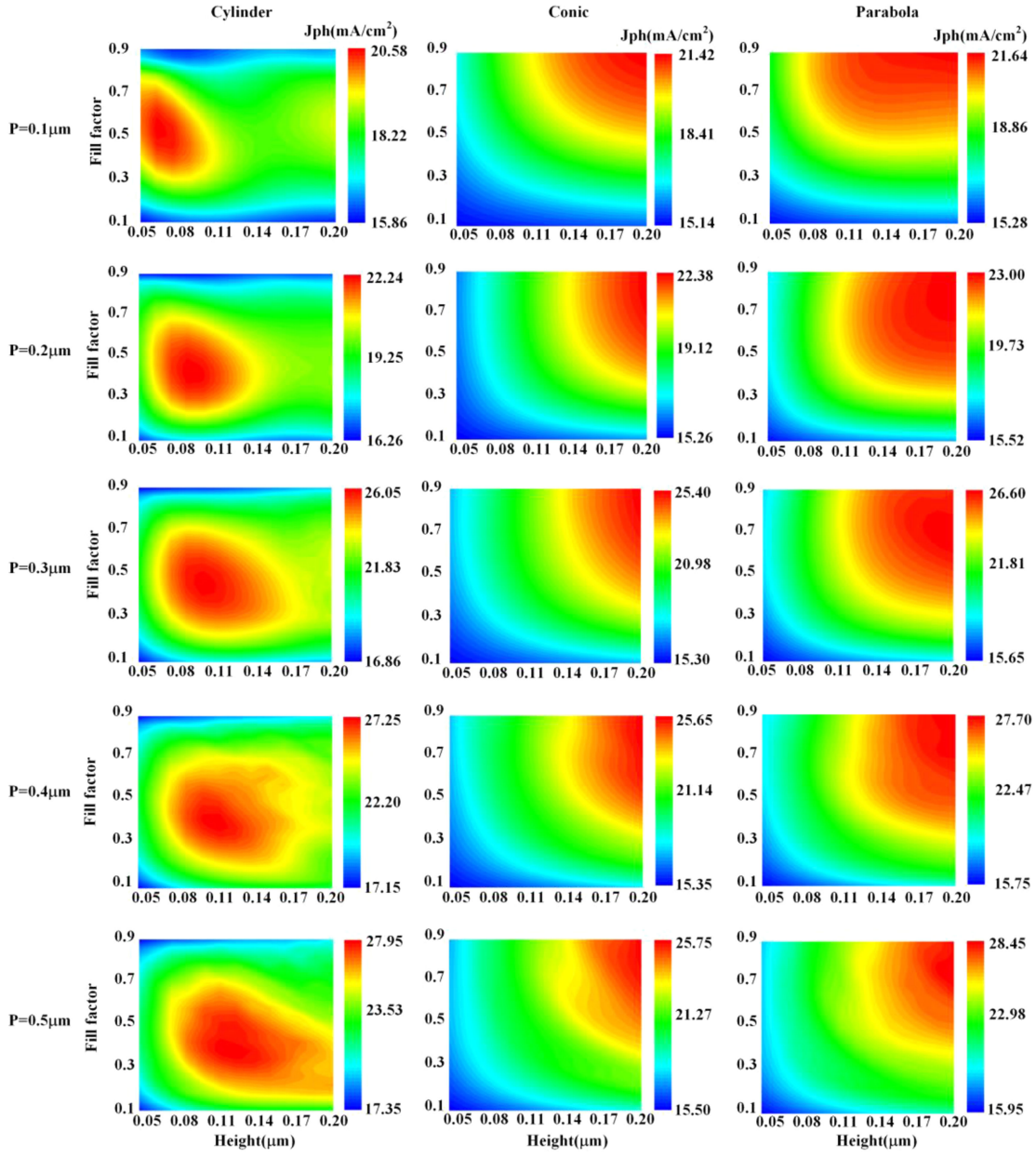

Fig. 2. Relationships between nanostructured parameters and Jph of solar cell at different periods. Height range is 0.05 μm $-$ 0.2 μm and the step size is 12.5 nm. Fill factor ranges from 0.1 to 0.9 with a step size of 0.04.

As shown in Fig. 2, the values of Jph show close dependency to the architecture parameters of the nanostructure applied. When the period changes from 0.1 μm to 0.5 μm, one can easily observe that for all these three models: (1) the maximum value of the Jph shows a positive dependency as the structure period increases; (2) the enhancement domain area (EDA, red color region in Fig. 2) goes bigger and shifts to the bottom-right direction (with a larger H and smaller F); (3) the boundary of the EDA becomes much more rough as the period grows, which may be induced from the enhanced scatter effect from a bigger nanostructured dimension. Besides, for a specific nanostructured period (e.g., P $=$ 0.2 μm), the areas of the EDA for CCN and PBN ones have

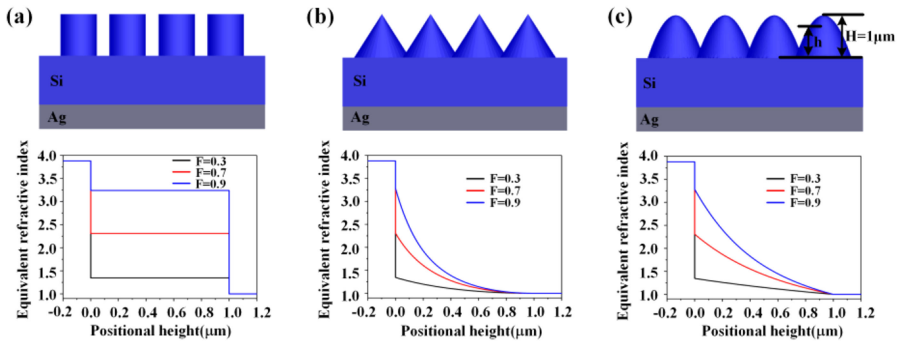

Fig. 3. The equivalent refractive index profile of (a) CDN arrays, (b) CCN arrays and (c) PBN arrays. The refractive index of the c-Si was obtained at wavelength of 0.633 μm, and the fill factors are defined by the value at the starting point (0 μm) of each nanostructured array.

been enlarged, (which has been further confirmed by Fig. 4) indicating a less sensitive property to structure height and fill factor when comparing to the CDN one. Actually, this result could be of great importance for the design and fabrication of the nanostructure based solar cells, because it is really hard to precisely control the structure dimension in the practical application when feature size decreases down to nanometer scale. Under such consideration, the advantages by using CCN and PBN can be fully exhibited. Due to the limitation of the calculation ability, only limited dimension range is shown in Fig. 2, the detailed light trapping properties of these three nanostructures based solar cells will be further discussed in the subsequent sections.

Equivalent refractive index provided by reasonable fill factor of nanostructure has good antireflection effect [39]. Therefore, the relationship between the height of nanostructure and Jph was further studied based on fill factors. Take the period of 0.5 as an example, the equivalent refractive indices of three nanostructures are plotted at different positional heights, as shown in Fig. 3. The variation of the equivalent refractive index of the cylinder in Fig. 3(a) with the height position is given by the following equation [43]:

$$(1-f)\frac{n_{si}^2-n_{air}^2}{n_{si}^2-n_{eff}^2}=\frac{n_{air}}{n_{eff}} \tag{3}$$

where n_{Si} is the refractive index of silicon, n_{air} is the refractive index of air, n_{eff} and f are respectively the equivalent refractive index and fill factor of the nanostructure at different positions. The variation of equivalent refractive index with positional height h in Fig. 3(b) and (c) can be given by simply putting function $r_1 = (H - h) \bullet r/H$ and $r_2 = r \bullet \sqrt{1 - h/H}$ (r_1 and r_2 are the radii of CCN and PBN at h, respectively.) into the above equation:

$$\left[1-\frac{2\pi\left(\frac{H-h}{H}r\right)^2}{A}\right]\frac{n_{si}-n_{air}}{n_{si}-n_{eff}}=\frac{n_{air}}{n_{eff}} \tag{4}$$

$$\left\{1-\frac{2\pi\left[\left(\sqrt{1-\frac{h}{H}}\right)r\right]^2}{A}\right\}\frac{n_{si}-n_{air}}{n_{si}-n_{eff}}=\frac{n_{air}}{n_{eff}} \tag{5}$$

where h is the positional height, A is the area of the smallest repeating unit of the nanostructure, H is the height of the nanostructure and r is the radius of the nanostructure at the bottom position. The surface nanostructure can effectively improve the external quantum efficiency of LED and solar cell because of an architecture with gradually changed refractive index from the bulk layer to the nanostructured layer [44], [45]. Therefore, for the CCN and PBN, as shown in Fig. 3(b) and Fig. 3(c), the bigger the fill factor is, the much smoother the equivalent refractive index along the positional

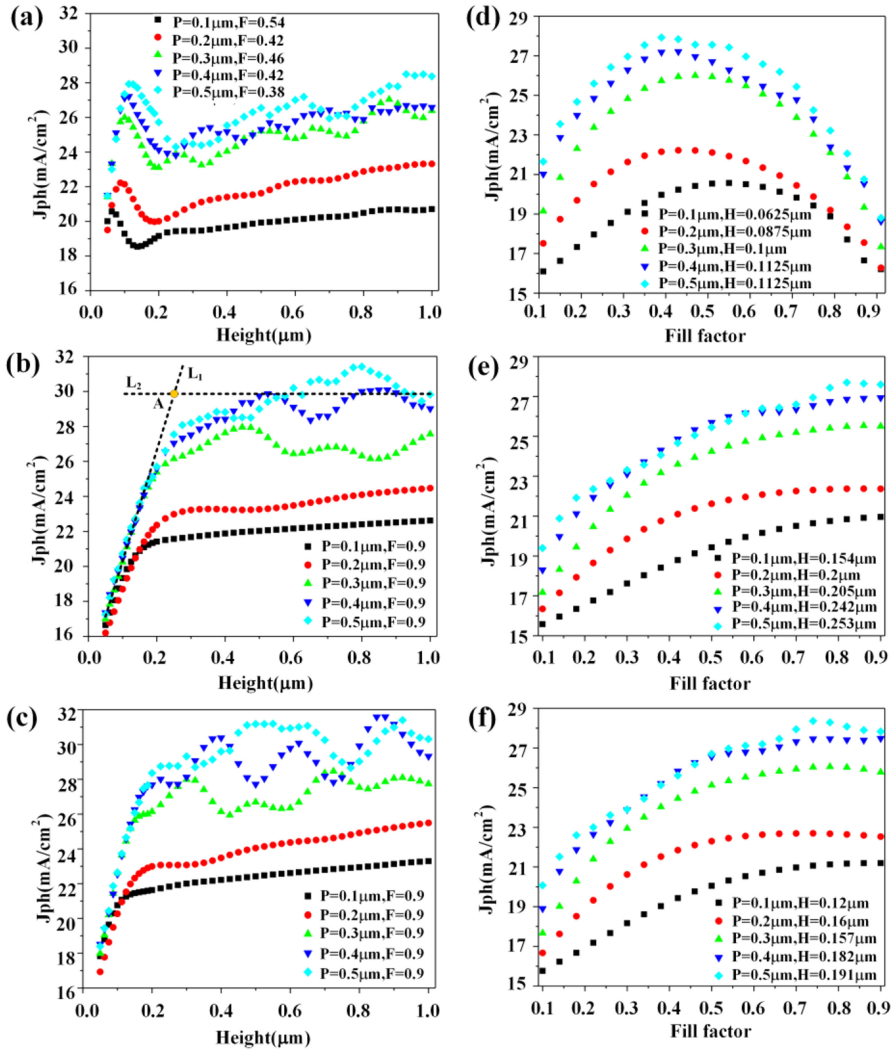

Fig. 4. The relationship between Jph and the height of nanostructure for (a) cylindrical, (b) conical and (c) parabolic nanostructure. (d), (e) and (f) are the corresponding relationship between Jph and fill factor of (a), (b) and (c), respectively. The H in Fig. 4 (d) is the height of Jph peak from the range of 0.05 μm to 0.2 μm in Fig. 4 (a). In Fig. 4(e) and Fig. 4(f), the H is the height value that the point of intersection belongs to. Take point A in Fig. 4(b) for example, the L1 is the linear variation of the Jph at height ranges from 0.05 μm to 0.2 μm and the L2 is the average value of Jph during the height of 0.25 μm to 1 μm as shown in Fig. 4(b). These two lines intersect at point A and finally defines the height value under period of 0.5 μm in Fig. 4(e).

height will be. Under such consideration, the optimum fill factor for CCN and PBN can be chosen at 0.9, which corresponds to the situation when two adjacent nanostructures are close enough to each other and about to overlap. As for the CDN arrays, the $\lambda/4$ single film effect will dominate and shows a strong height dependent tendency as shown in Fig. 2. The CDN array has the optimum fill factor and height when Jph is the largest. Nevertheless, the optimum fill factor and height are different under diverse periods. Hence, we selected different optimum fill factors for each perioded CDN arrays in Fig. 4(a) as to study the height dependent properties.

When the H of the nanostructure is less than 0.2 μm, the CDN has a Jph peak appears in every period as shown in Fig. 4(a), which can be explained by thin film theory [46]. According to the thin

TABLE 1
Maximum Jph of Nanostructured Solar Cells

Nanostructure-type	Fill factor	Height (μm)	Period(μm)	Jph of maximum (mA/cm^2)
Parabola	0.9	0.875	0.4	31.593
Cone	0.9	0.8	0.5	31.414
Cylinder	0.38	0.925	0.5	28.5

film theory, when $n_{eff} = \sqrt{n_{air} n_{si}}$ and the thickness h of the thin film satisfies:

$$n_{eff} h = (2m+1)\frac{\lambda}{4} (m = 0, 1, 2 \ldots) \tag{6}$$

the film has the best antireflection performance. With respect to Fig. 4(b) and Fig. 4(c), for CCN and PBN with the gradient equivalent refractive index, the Jph increases approximately linearly with the nanostructure height at a lower H range (e.g., H $<$ 0.2 μm for the CCN when P equals to 0.5 μm, as shown by the dashed line L1 in Fig. 4(b)). When the H is 0.2 μm to 1 μm, the Jph tend to increase with H, and produce a distinct oscillation at the period more than 0.3 μm, but the oscillation trend of CCN and PBN is relatively stable because of a uniform change of equivalent refractive index. The relationship between Jph and fill factor of these three nanostructures is illustrated in Fig. 4(d)–(f). The CDN has a maximum Jph for each period in Fig. 4(d), since they can always provide an equivalent refractive index that compliance with the $\lambda/4$ thin film theory at a reasonable light wavelength. Fig. 4(e) and Fig. 4(f) show that with the increase of fill factor the Jph value becomes bigger. In addition, because the CCN and PBN have more uniform gradient refractive index, the Jph curve becomes much more stable and smoother along with the increase of fill factor, and a maximum value is obtained near the fill factor of 0.9.

Throughout Fig. 4, the increase of the period and height of nanostructure results in high-order diffraction and scattering enhancement [14], [22], which makes the Jph increase and produces oscillation. Comparing Fig. 4(a), 4(b) and 4(c), it can be seen that they have better results under a larger H because the equivalent absorption volume of silicon is increasing. The maximum values of Fig. 4 are described in Table 1. Although when the H is less than 0.2 μm, the CDN also has a sharp peak of Jph, it has a strong dependence on H. Similarly, in Fig. 4(d), 4(e) and 4(f), the Jph of CDN has a peak value with the change of fill factor, which indicates that Jph of CDN is also much more sensitive to the fill factor than the other two structures. The above discussion is consistent with the conclusion in Fig. 2 section. Furthermore, one cannot make the height of the nanostructure as high as possible since the thickness of the ultra-thin solar cell has already limited in real applications. For the same reason, the method mentioned in Fig. 4 was used to balance the H value and the desired Jph for the CCN and PBN solar cells. Consequently, Table 2 lists the optimized Jph of nanostructured and AR layered solar cells under the limited height of less than 0.26 μm for the consideration of practical applications.

In Table 2, to reduce the absorption influence from unequal volume the material, the silicon volume of the AR (anti-reflective) layered solar cell is set to be the same as that of the nanostructured one, the effective volume thickness of the silicon for AR layered solar cells corresponding to cylindrical, conical and parabolic solar cells are 1.043 μm, 1.076 μm and 1.09 μm, respectively. The AR layer is Si_3N_4 with optimized thickness of 0.06 μm [47]. As shown, all the three nanostructured solar cells obtain an efficiency enhancement as high as more than 33% even with a limited structure height less than 0.26 μm around. Although the enhancements of these three nanostructures are

TABLE 2
Optimized Jph of Nanostructured and AR Planar Solar Cells Under the Same Volume

Nanostructure-type	Fill factor	Height (μm)	Nanostructured Jph (mA/cm^2)	AR layered Jph (mA/cm^2)	Enhancing efficiency
Parabola	0.9	0.191	28.04	20.9	34.2%
Cone	0.9	0.253	27.596	20.753	33%
Cylinder	0.38	0.1125	27.927	20.453	36.5%

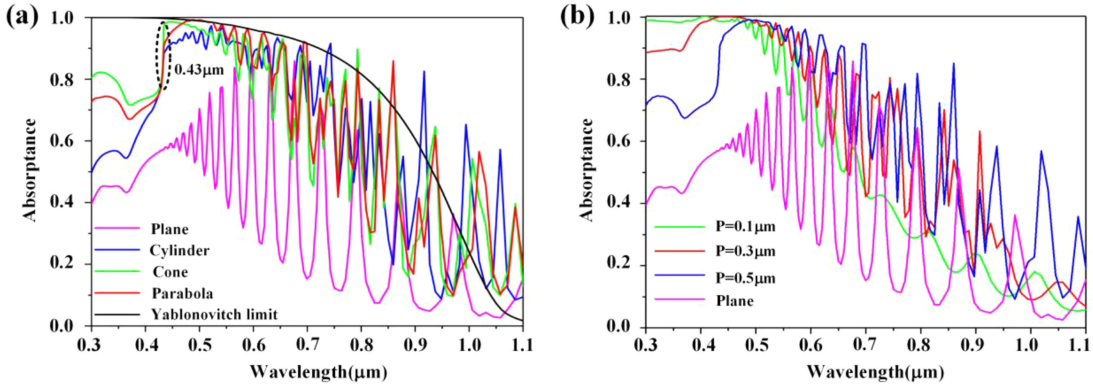

Fig. 5. (a) Absorptance calculation results for a 1 μm thick solar cell with and without nanostructure. CDN at P = 0.5 μm, f = 0.38, H = 112.5 nm; CCN at P = 0.5 μm, f = 0.9, H = 253 nm; PBN at P = 0.5 μm, f = 0.9, H = 191 nm. The absorptance of Yablonovitch light capture limit of 1 μm thick c-Si is used for reference. (b) The impact of period parameters to the spectral dependent absorbance (e.g., PBN, f = 0.9, H = 191 nm).

comparable, Jph for the CCN and PBN ones have little dependence on H and F, which brings great convenience to the real application of corresponding devices.

According to formula (1), the increase of Jph means a strong absorption. Fig. 5 displays the absorptance of the nanostructured and planar ultra-thin c-Si with thickness of 1 μm. The Yablonovitch limit is expressed as [48]–[50]:

$$A_b = 1 - \frac{1}{1 + 4n^2 \alpha d} \tag{7}$$

where n is the real part of the refractive index of the material, α is the absorption coefficient, and d is the thickness of the absorption layer. Due to surface nanostructure introduced multiple effects including destructive wave interference, total internal reflection and scattering [51], the absorptance of solar cells can be greatly enhanced as shown in Fig. 5(a). In the wavelength range of 0.3–0.471 μm, the CCN has the best light capturing ability. While the absorption of CCN solar cell decreases gradually, and begins to be smaller than that of the CDN one at the wavelength of 0.54 μm, which explains why the efficiency enhancement of Jph of the CCN one is slightly smaller than that of the CDN one. Similar conclusion can be drawn for the PBN. For the same reason, the resonances of the CCN and PBN solar cells start a little behind the CDN one because of a higher absorption in shorter wavelength and thus less light will be reflected back and dedicated to the interference at the top interfaces. It can be seen that when the wavelength is longer than 0.45 μm, a resonance of the spectrum can be easily observed. This is because in the short wavelength range, the silicon has a very strong absorption coefficient and all the light get into the silicon

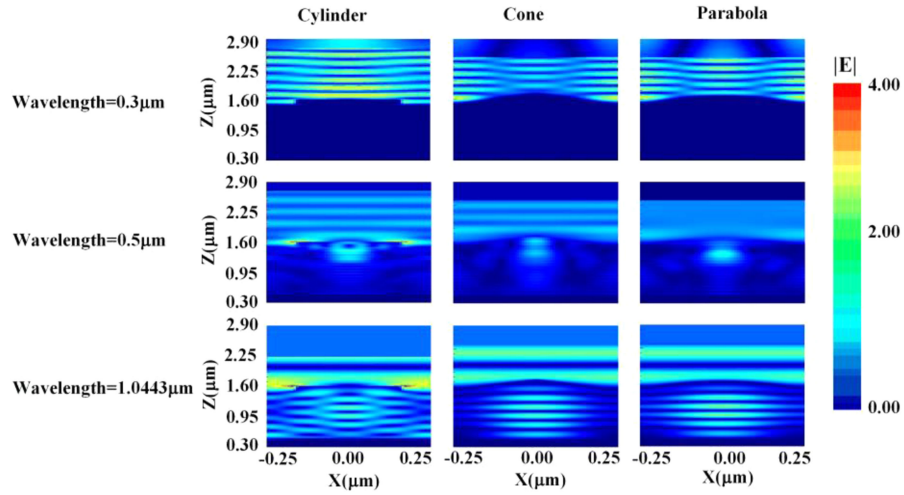

Fig. 6. At normal incidence, the electric field distribution at the X-Z cut of the CDN, CCN and PBN solar cells at wavelengths of 0.3 μm, 0.5 μm and 1.0443 μm.

slab will be absorbed totally, thus no light will be reflected back to make the interference at the front surface. While for the long wavelength range, it's just the opposite. Moreover, benefit from the excellent antireflection property of the surface nanostructure, the resonance peaks induced at the wavelength range of 0.80–1.1 μm breaks the Yablonovitch limit as shown in Fig. 5(a). One may notice that the curves for the nanostructured solar cells show an obvious raising step at around 0.43 μm in Fig. 5(a). This sharp step is only related to the period, therefore, we consider that the first-order diffraction is satisfied, which makes the diffractive light absorbed completely. Nevertheless, in the study, we found that the absorption behavior of the wavelength shows a very strong dependence upon the period of the nanostructures. As shown in Fig. 5(b), for the nanostructured solar cell with period of 0.1 μm shows a better absorption performance in short wavelength range but a worse behavior in the long wavelength part compared to these with a bigger period (p $=$ 0.3 μm and p $=$ 0.5 μm). Actually, the smaller the period of the nanostructured solar cell is, the better the absorption performance in short wavelength will be. For the situation in long wavelength part, it is the opposite.

The mechanism of light capture ability of nanostructured solar cell was studied by their electric field at 0.3 μm, 0.5 μm and 1.0443 μm. The distribution of the electric field strength is shown in Fig. 6. It can be seen that in the short wavelength region (e.g., 0.3 μm), nanostructure provide Mie scattering resonance to enhance the absorption performance [52], [53], but strong surface reflection limits the increase of absorption. In the mid-band (e.g., 0.5 μm), besides the weak Mei scattering resonance and F-P resonance, the first-order diffraction of nanostructure also provides a strong optical waveguide mode, which greatly improves the absorption capacity of c-Si [54], [55]. Therefore, the absorption layer has the best electric field distribution and absorption. At the long wavelength (e.g., 1.0433 μm), the guided mode disappears in c-Si, while the enhanced Mie scattering resonance, the F-P resonance still exist, thus ensures an enhanced absorption at the long wavelength band.

To characterize the parasitic absorption of the Ag mirror, the Ag mirror of Fig. 1 is replaced by PEC (perfect electric conductor). The corresponding results are shown in Fig. 7, which uses optimized parabolic nano-structure as an example. As shown, only 0.36 mA/cm^2 of Jph difference can be obtained and almost no surface plasmon excitation at the Si/Ag interface can be observed. Thus, the decrease in absorptance is mainly caused by parasitic absorption of Ag mirror [8], but it has little effect on the overall silicon absorption as shown in Fig. 7. Therefore, the strategy has great flexibility in material choice for either the surface nanostructure or the back-reflector. Here, one

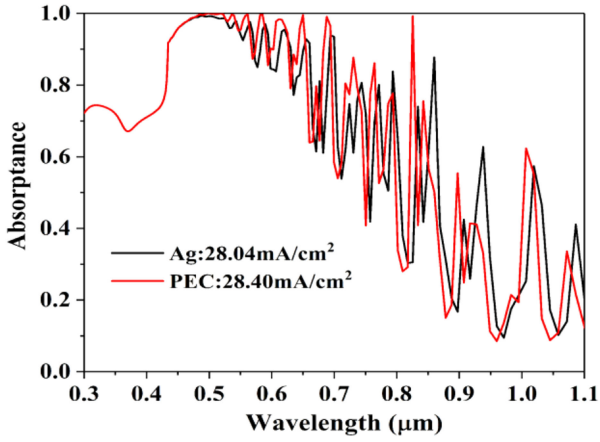

Fig. 7. The absorption spectra with Ag and PEC.

should notice that, the parasitic absorption of Ag contact has no contribution to the photocurrent generation and has been excluded from all simulations since the red rectangle area in Fig. 1 only monitors the absorption fraction from silicon. For the same reason, the PEC model in Fig. 7 has a higher Jph than that of the Ag model.

4. Conclusion

In summary, we applied nanostructures with cylindrical, conical and parabolic sidewall profiles based on AAO to the surface of ultra-thin solar cells, and studied the light trapping abilities of the corresponding nanostructures. The results show that the Jph improves with the increasing of nanostructured period from 0.1 μm to 0.5 μm. In the meanwhile, the efficient light trapping area (defined by F$\times$H) of the nanostructured solar cell can be effectively enlarged. The conical and parabolic nanostructures are insensitive to the structural parameters (H from 0.05 μm to 1 μm and fill factor from 0.1 to 0.9) while ensuring high performance. We considered the preparation process of nanostructures, the thickness of ultra-thin solar cells and optimized parameters with respect to the practical applications. The enhancements of light absorption of solar cells in full wavelength range were attributed to the equivalent refractive index of nanostructures, so that their Jphs have been upgraded by more than 33% compared with that of the AR planar solar cell. This study is of great help for the design and optimization of sidewall profile dependent high performance nanostructured ultrathin solar cells.

References

[1] T. D. Lee and A. U. Ebong, "A review of thin film solar cell technologies and challenges," *Renew. Sustain. Energy Rev.*, vol. 70, pp. 1286–1297, 2017.
[2] S. Moon, K. Kim, Y. Kim, J. Heo, and J. Lee, "Highly efficient single-junction GaAs thin-film solar cell on flexible substrate," *Scientific Rep.*, vol. 6, 2016, Art. no. 30107.
[3] L. C. Andreani, A. Bozzola, and M. Liscidini, "The importance of light trapping in thin-film solar cells," SPIE Newsroom, pp. 1–2, 2012.
[4] S. Lee and S. Kim, "Optical absorption characteristic in thin a-Si film embedded between an ultrathin metal grating and a metal reflector," *IEEE Photon. J.*, vol. 5, no. 5, Oct. 2013, Art. no. 4800610.
[5] T. Sun, Z. Xu, H. Xu, W. Zhao, and J. Peng, "Direct tailoring the Si substrate for antireflection via random nanohole nanoimprint," *J. Nanosci. Nanotechnol.*, vol. 15, no. 2, pp. 1297–1303, 2015.
[6] H. P. Wang *et al.*, "Photon management in nanostructured solar cells," *J. Mater. Chem. C*, vol. 2, no. 17, pp. 3144–3171, 2014.
[7] V. K. Narasimhan and Y. Cui, "Nanostructures for photon management in solar cells," *Nanophoton.*, vol. 2, no. 3, pp. 187–210, 2013.
[8] W. Ken Xingze, Y. Zongfu, L. Victor, C. Yi, and F. Shanhui, "Absorption enhancement in ultrathin crystalline silicon solar cells with antireflection and light-trapping nanocone gratings," *Nano Lett.*, vol. 12, no. 3, pp. 1616–1619, 2012.

[9] Y. H. Ye, C. C. Chin, and D. W. Huang, "Enhanced conversion efficiency for solar cells with periodic grating of nanowires," *IEEE Photon. J.*, vol. 5, no. 5, Oct. 2013, Art. no. 8400709.
[10] Y. F. Li, L. Yue, Y. N. Luo, W. J. Liu, and M. C. Li, "Light harvesting of silicon nanostructure for solar cells application," *Opt. Express*, vol. 24, no. 14, 2015, Art. no. A1075.
[11] G. X. Ren *et al.*, "High efficiency organic solar cells achieved by the simultaneous plasmon-optical and plasmon-electrical effects from plasmonic asymmetric modes of gold nanostars," *Small*, vol. 12, no. 37, pp. 5200–5207, 2016.
[12] W. C. H. Choy and X. G. Ren, "Plasmon-electrical effects on organic solar cells by incorporation of metal nanostructures," *IEEE J. Sel. Top. Quantum Electron.*, vol. 22, no. 1, Jan./Feb. 2016, Art. no. 4100209.
[13] Q. Lin *et al.*, "Scalable indium phosphide thin-film nanophotonics platform for photovoltaic and photoelectrochemical devices," *ACS Nano*, vol. 11, no. 5, pp. 5113–5119, 2017.
[14] T. K. Chong, J. Wilson, S. Mokkapati, and K. R. Catchpole, "Optimal wavelength scale diffraction gratings for light trapping in solar cells," *J. Opt.*, vol. 14, no. 2, 2012, Art. no. 024012.
[15] R. Liu *et al.*, "Silicon nanowire/polymer hybrid solar cell-supercapacitor: A self-charging power unit with a total efficiency of 10.5%," *Nano Lett.*, vol. 17, no. 7, pp. 4240–4247, 2017.
[16] S. Jeong, M. D. Mcgehee, and Y. Cui, "All-back-contact ultra-thin silicon nanocone solar cells with 13.7% power conversion efficiency," *Nature Commun.*, vol. 4, 2013, Art. no. 2950.
[17] Y. R. Huang *et al.*, "Light extraction efficiency enhancement of flip-chip blue light-emitting diodes by anodic aluminum oxide," *Beilstein J. Nanotechnol.*, vol. 9, no. 1, pp. 1602–1612, 2018.
[18] H. F. Xu *et al.*, "Porous light-emitting diodes with patterned sapphire substrates realized by high-voltage self-growth and soft UV nanoimprint processes," *J. Lightw. Technol.*, vol. 32, no. 2, pp. 326–332, 2013.
[19] K. H. Tsui *et al.*, "Low-cost, flexible, and self-cleaning 3D nanocone anti-reflection films for high-efficiency photovoltaics," *Adv. Mater.*, vol. 26, no. 18, pp. 2805–2811, 2014.
[20] C. Zhang, L. Chen, Y. Zhu, and Z. Guan, "Fabrication of 20.19% efficient single-crystalline silicon solar cell with inverted pyramid microstructure," *Nanoscale Res. Lett.*, vol. 13, no. 1, 2018, Art. no. 91.
[21] Q. Lin *et al.*, "High performance thin film solar cells on plastic substrates with nanostructure-enhanced flexibility," *Nano Energy*, vol. 22, pp. 539–547, 2016.
[22] X. Wang *et al.*, "Improved optical absorption in visible wavelength range for silicon solar cells via texturing with nanopyramid arrays," *Opt. Express*, vol. 25, no. 9, pp. 10464–10472, 2017.
[23] H. Masuda and K. Fukuda, "Ordered metal nanohole arrays made by a two-step replication of honeycomb structures of anodic alumina," *Science*, vol. 268, no. 5216, pp. 1466–1468, 1995.
[24] H. Deniz, T. Khudiyev, F. Buyukserin, and M. Bayindir, "Room temperature large-area nanoimprinting for broadband biomimetic antireflection surfaces," *Appl. Phys. Lett.*, vol. 99, no. 18, 2011, Art. no. 183107.
[25] A. Beltiukov, E. Stashkova, and O. Boytsova, "Anodic oxidation of Al/Ge/Al multilayer films," *Appl. Surf. Sci.*, vol. 459, pp. 583–587, 2018.
[26] B. Dudem, J. W. Leem, and J. S. Yu, "A multifunctional hierarchical nano/micro-structured silicon surface with omnidirectional antireflection and superhydrophilicity via an anodic aluminum oxide etch mask," *RSC Adv.*, vol. 6, no. 5, pp. 3764–3773, 2016.
[27] W. Zhou, J. Zhang, X. Li, Y. Liu, and G. Min, "Replication of mold for UV-nanoimprint lithography using AAO membrane," *Appl. Surf. Sci.*, vol. 255, no. 18, pp. 8019–8022, 2009.
[28] W. M. Zhou, G. Q. Min, Z. T. Song, J. Zhang, Y. b. Liu, and J. P. Zhang, "Enhanced efficiency of light emitting diodes with a nano-patterned gallium nitride surface realized by soft UV nanoimprint lithography," *Nanotechnology*, vol. 21, no. 20, 2010, Art. no. 205304.
[29] T. Sun *et al.*, "Photonic crystal structures on nonflat surfaces fabricated by dry lift-off soft UV nanoimprint lithography," *J. Micromech. Microeng.*, vol. 23, no. 12, 2013, Art. no. 125002.
[30] Y. Cho, H. K. Minsky, Y. Jiang, K. Yin, K. T. Turner, and S. Yang, "Shear adhesion of tapered nanopillar arrays," *ACS Appl. Mater. Interfaces*, vol. 10, no. 13, pp. 11391–11397, 2018.
[31] Z. Zhang *et al.*, "The fabrication of the antireflective periodic nano-arrary structure on Si surface using nanoimprint lithography and the study on its properties," *Acta Phys. Sinica*, vol. 62, no. 16, 2013, Art. no. 168102.
[32] K. Choi *et al.*, "Nano-tailoring the surface structure for the monolithic high-performance antireflection polymer film," *Adv. Mater.*, vol. 22, no. 33, pp. 3713–3718, 2010.
[33] E. D. Palik, "*Handbook of Optical Constants of Solids I-III*. New York, NY, USA: Academic, 1991.
[34] D. R. Lide, *Handbook of Chemistry and Physics*. Boca Raton, FL, USA: CRC Press, 1998.
[35] A. P. Li, F. Muller, A. Birner, K. Nielsch, and U. Gosele, "Hexagonal pore arrays with a 50–420 nm interpore distance formed by self-organization in anodic alum," *J. Appl. Phys.*, vol. 84, no. 11, pp. 6023–6026, 1998.
[36] I. Mínguez-Bacho, F. Scheler, P. Büttner, K. Bley, N. Vogel, and J. Bachmann, "Ordered nanopore arrays with large interpore distances via one-step anodization," *Nanoscale*, vol. 10, no. 18, pp. 8385–8390, 2018.
[37] H. Li *et al.*, "Morphology-dependent high antireflective surfaces via anodic aluminum oxide nanostructures," *Appl. Surface Sci.*, vol. 496, Dec. 2019, Art. no. 143697, doi: 10.1016/j.apsusc.2019.143697.
[38] H. Lin *et al.*, "Rational design of inverted nanopencil arrays for cost-effective, broadband, and omnidirectional light harvesting," *ACS Nano*, vol. 8, no. 4, pp. 3752–3760, 2014.
[39] J. Zhu, Z. Yu, S. Fan, and Y. Cui, "Nanostructured photon management for high performance solar cells," *Mater. Sci. Eng.: R: Rep.*, vol. 70, no. 3–6, pp. 330–340, 2010.
[40] Y. Lei, M. Yuan, D. Yang, and D. Li, "Unidirectional light scattering by up-down Janus dimers composed of gold nanospheres and silicon nanorods," *Opt. Commun.*, vol. 435, pp. 362–366, 2019.
[41] Z. Yang *et al.*, "Broadband and wide-angle light harvesting by ultra-thin silicon solar cells with partially embedded dielectric spheres," *Opt. Lett.*, vol. 41, no. 7, pp. 1329–1332, 2016.
[42] M. Hamdy, M. F. O. Hameed, and S. S. A. Obayya, "Broadband absorption enhancement in modified grating thin-film solar cell," *IEEE Photon. J.*, vol. 9, no. 3, Jun. 2017, Art. no. 2700314.
[43] D. Ranguin, "Subwavelength structured surfaces: Theory and application," Ph. D. dissertation, University of Rochester, Rochester, NY, USA, 1993.

[44] Z. Chi *et al.*, "Efficient and flexible thin film amorphous silicon solar cells on nanotextured polymer substrate using sol–gel based nanoimprinting method," *Adv. Functional Mater.*, vol. 27, no. 13, 2017, Art. no. 1604720.
[45] S. Baek, G. Kang, D. Shin, K. Bae, H. K. Yong, and K. Kim, "Improvement of light extraction efficiency in flip-chip light emitting diodes on SiC substrate via transparent haze films with morphology-controlled collapsed alumina nanorods," *ACS Appl. Mater. Interfaces*, vol. 8, no. 1, pp. 135–141, 2016.
[46] W. Lei, H. Zhang, F. Qin, X. Bai, Z. Ji, and H. Dan, "Performance enhancement of pc-Si solar cells through combination of anti-reflection and light-trapping: Functions of AAO nano-grating," *Opt. Commun.*, vol. 385, pp. 205–212, 2017.
[47] K. Luke, Y. Okawachi, M. R. E. Lamont, A. L. Gaeta, and M. Lipson, "Broadband mid-infrared frequency comb generation in a Si_3N_4 microresonator," *Opt. Lett.*, vol. 40, no. 21, pp. 4823–4826, 2015.
[48] M. A. Green, "Lambertian light trapping in textured solar cells and light-emitting diodes: Analytical solutions," *Prog. Photovolt. Res. Appl.*, vol. 10, no. 4, pp. 235–241, 2010.
[49] A. Bozzola, M. Liscidini, and L. C. Andreani, "Photonic light-trapping versus Lambertian limits in thin film silicon solar cells with 1D and 2D periodic patterns," *Opt. Express*, vol. 20, no. S2, pp. A224–A244, 2012.
[50] S. E. Han and G. Chen, "Toward the Lambertian limit of light trapping in thin nanostructured silicon solar cells," *Nano Lett.*, vol. 10, no. 11, pp. 4692–4696, 2010.
[51] X. G. Ren, X. C. Li, and W. C. H. Choy, "Optically enhanced semi-transparent organic solar cells through hybrid metal/nanoparticle/dielectric nanostructure," *Nano Energy*, vol. 17, pp. 187–195, 2015.
[52] S. Zhong, W. Wang, Y. Zhuang, Z. Huang, and W. Shen, "All-solution-processed random Si nanopyramids for excellent light trapping in ultrathin solar cells," *Ad. Funct. Mater.*, vol. 26, no. 26, pp. 4768–4777, 2016.
[53] H. Ren, X. Ren, Z. Huang, and X. Wu, "Synergetic light trapping effects in organic solar cells with a patterned semi-transparent electrode," *Phys. Chem. Chem. Phys.*, vol. 21, no. 21, pp. 11306–11312, 2019.
[54] Y. Lin *et al.*, "Dual-layer nanostructured flexible thin-film amorphous silicon solar cells with enhanced light harvesting and photoelectric conversion efficiency," *ACS Appl. Mater. Interfaces*, vol. 8, no. 17, pp. 10929–10936, 2016.
[55] M. L. Brongersma, Y. Cui, and S. H. Fan, "Light management for photovoltaics using high-index nanostructures," *Nature Mater.*, vol. 13, no. 5, pp. 451–460, 2014.